Received 20 May 2024; accepted 10 September 2024. Date of publication 16 September 2024; date of current version 20 September 2024.
The review of this article was arranged by Editor J. Kumar.

Digital Object Identifier 10.1109/JEDS.2024.3461169

Combining Intelligence With Rules for Device Modeling: Approximating the Behavior of AlGaN/GaN HEMTs Using a Hybrid Neural Network and Fuzzy Logic Inference System

AHMAD KHUSRO, SADDAM HUSAIN, AND MOHAMMAD S. HASHMI (Senior Member, IEEE)

School of Engineering and Digital Sciences, Nazarbayev University, 010000 Astana, Kazakhstan

CORRESPONDING AUTHOR: M. S. HASHMI (e-mail: mohammad.hashmi@nu.edu.kz)

This work was supported by the Science Committee of the Ministry of Science and Higher Education of the Republic of Kazakhstan, under Grant AP23489460.

ABSTRACT This paper uses the Adaptive Neuro-Fuzzy Inference System (ANFIS) to investigate and propose a new alternative behavioral modeling technique for microwave power transistors. Utilizing measured I-V characteristics, associated parameters like transconductance (g_m) and output conductance (g_{ds}), etc., S-parameters characteristics, and RF performance parameters such as unity current gain frequency (f_T), maximum unilateral gain frequency (f_{max}), ANFIS-based behavioral models are developed for Gallium Nitride (GaN) High Electron Mobility Transistors (HEMTs) and validated. The models have been developed using two distinct devices with dimensions of $10 \times 200\ \mu m$ and $10 \times 250\ \mu m$ for multi-bias conditions and over a broad frequency range (0.5 to 43.5 GHz). Subsequently, the proposed model performance is validated on devices with geometries of $10 \times 220\ \mu m$, $4 \times 100\ \mu m$, and $2 \times 200\ \mu m$ to examine the interpolation accuracy, extrapolation potential, and scalability. Here, ANFIS utilizes the subtractive clustering method to process the measurement characteristics by computing the clusters and opts for the best-performing model using error and number of fuzzy rules as criteria. The parameters involved in the fuzzy representation are trained using neural network algorithms, namely gradient-descent and least squares estimate. The proposed models are subsequently incorporated in a commercial circuit simulator (Keysight's ADS) and the class-F power amplifier's gain and stability characteristics are computed and studied.

INDEX TERMS GaN HEMTs, artificial intelligence, ANFIS, behavioral device modeling, fuzzy logic, neural networks, RF power amplifiers.

I. INTRODUCTION

The requirements of advanced wireless standards have resulted in several innovations in the past two decades in the domain of Radio Frequency (RF)/Microwave circuits, components, and systems [1], [2], [3], [4]. It is imperative to note that the design of active circuits faces more stringent challenges due to the limitations of the transistor device models. For example, the design of RF Power Amplifiers (PAs) is heavily dependent on the availability of active device models. In this context, there has been immense emphasis on the use of Gallium Nitride (GaN) High Electron Mobility Transistors (HEMTs) considering its unique set of features, for RFPAs designs. However, available GaN HEMT models are limited, hence new modeling techniques for GaN HEMT model development are extremely critical.

Research on GaN HEMT modeling has been essential for its potential application in high-power and high-frequency transceiver design [5], [6]. This has been made possible owing to the unique traits of GaN HEMTs such as wide energy band gap, high electron saturation velocity, high breakdown voltage, and high-frequency operation. Numerous techniques for modeling GaN HEMTs have been widely

reported and can be segregated basically into three categories: (i) physics-based model; (ii) empirical-based model and (iii) Behavioral model. The roots and foundations of physics/compact-based models lie behind physical equations, analytical frameworks, and theoretical concepts. For example, the Advanced Spice Model (ASM) for HEMTs is a surface potential model developed using Schrodinger and Poisson's equations [7], [8], [9], [10], [11], whereas MIT Virtual Source GaN (MVSG) is a charge-based physical model [12], [13], [14], [15]. The second technique is an empirical modeling approach such as the Angelov model or cold pinch-off-based parameter extraction approach, which makes use of heuristics, empirical equations to characterize the non-linear components, experimental methods, and curve fitting to model the devices [16], [17], [18], [19], [20], [21], [22], [23]. The empirical approach has a simple extraction flow but is not suitable and reliable for large signal conditions in many cases as it is extracted from S-parameters and lacks scalability as well. While these techniques are highly precise and accurate, they are computationally inefficient and cumbersome. Recently, ML-based techniques such as Artificial Neural Network (ANN), Support Vector Regression (SVR), Gaussian Process Regression (GPR), Decision Trees (DTs) have gained prominence in the device modeling domain owing to their accuracy and quick turnaround time [24], [25], [26], [27], [28], [29], [30], [31], [32], [33], [34]. ML-based models optimize hyperparameters (modeling parameters of the corresponding models) for accurate fitting, modeling, and prediction. For example, the ANN algorithm optimizes hyperparameters such as weights and biases, activation functions, number of hidden layers, and associated neurons. In contrast, SVM emphasizes optimizing the regularization constant, epsilon width, and kernel function. Moreover, DT, a tree structure-based ML technique, optimizes the minimum number of leaves and the maximum number of splits to minimize the objective function error for accurate modeling of the devices. The number of these hyperparameters increases with the quantum of improvement the user envisages. In contrast to physics and empirical modeling, ML-based models offer design engineers an alternate strategy when only a few parameters need to be optimized. It also appears that developing device models more quickly and with pragmatic accuracy is a top concern. In addition, ML-based device models do not require explicit mathematical frameworks to achieve curve fitting and modeling accuracy. But unlike the other two methods, ML-based models have a principal drawback of the black-box approach, which is that it is still challenging to extract and understand structured knowledge and is not able to address issues such as scalability and accuracy over the extrapolation range. Amidst all the above modeling approaches, a new hybrid approach evolved for the development of device models - either by combining physics-based models with ML techniques [35], [36] or combining empirical-based models with ML techniques [37], [38]. These types of approaches exploit the potential of ML techniques and try to solve the scalability issue for empirical models and increase the degree and range of scalability for physics-based models as well.

Artificial Intelligence (AI) techniques are appealing and intriguing tools to solve non-linear and complex problems. Behavioral and hybrid approach-based device modeling fit well into these classes of problems. The fuzzy logic (FL) inference system belongs to one of the subsets of AI and its application within the domain of device modeling is extremely rare. Both neural networks and fuzzy systems are effective methods for solving complex problems. ANNs are computational models, capable of learning from vast amounts of data and are characterized by their ability to capture non-linear relationships and generalize from examples, making them highly suitable for developing behavioral models where the underlying relationships may not be easily represented by conventional mathematical models. On the other hand, FL allows reasoning and decision-making capability under uncertainty. Because FL follows linguistic principles, vague and imprecise information can be represented. Within a strong mathematical foundation, FL-based inference engines may convert expert knowledge into linguistic rules even in cases when the knowledge is lacking or uncertain. In some scenarios, FL-based models can be more useful than ML-based models, for the former can express the relationship between inputs and outputs in the inference process [39], [40]. However, it is important to mention that, in contrast to ML methods, the Fuzzy Inference System (FIS) lacks learning capabilities. The purpose is to harness the complementary strengths of both the approaches by integrating neural networks for adaptive learning and FL providing linguistic interpretation, decision-making based on the learned knowledge, and rule-based reasoning to effectively deal with multi-variable complex problems. Moreover, fuzzy-based models are highly immune to overfitting and provide better control over interpolation as well as extrapolation properties of the obtained mapping [40].

To study and investigate the use of an Adaptive Neuro-Fuzzy Inference System (ANFIS) in the behavioral device modeling domain, this paper employs a hybrid neuro-fuzzy technique that combines the benefits of fuzzy logic with neural networks. The proposed approach develops a rule-based inference engine for GaN HEMTs by mapping the inputs: devices of different geometries (number of fingers, unity gate, and effective gate width), the drain to source voltage (V_{DS}), the gate to source voltage (V_{GS}) and a broad frequency range) to the output space (I-V, S-parameters, and RF characteristics). A neuro-fuzzy approach works by developing an initial FIS created using a Subtractive Clustering (SC) algorithm, and subsequently optimizing the antecedent and consequent parts of the initial FIS to obtain a pragmatic improvement and gain in generalization capability of the proposed GaN HEMTs models. Data clustering algorithms aid in constructing FIS models from the measured data by segregating data into fuzzy subsets or clusters based on similarity between measured data [39], [40]. ANFIS approach represents the GaN HEMTs models by fuzzy

if-then rules, where the tuning parameters are updated by the neural network algorithms, Gradient Descent (GD) and Least Square Estimator (LSE) [41], [42]. Subsequently, the efficiency of the proposed models is tested on devices of geometries $10 \times 220\,\mu$m, $4 \times 100\,\mu$m and $2 \times 200\,\mu$m validating the interpolation and extrapolation potential. In addition, the scalability of the proposed model is also investigated. To the best knowledge of the authors, the proposed technique to model semiconductor devices is rarely reported in the literature. Furthermore, the ability to seamlessly incorporate the models into Computer-Aided Design (CAD) tools demonstrates the applicability of the developed models in RF circuit design. Below, we have summarized the advantages of the ANFIS-based GaN HEMTs models:

- Model performance does not scale down with the order of non-linearity involved in the measured characteristics;
- A short learning curve due to SC, good extrapolation capability, and excellent modeling performance on a testing device ($4 \times 100\,\mu$m and $2 \times 200\,\mu$m) demonstrates the scaling capability of the model;
- A robust model with no convergence issues owing to the hybrid algorithm;
- SC aids in obtaining a rugged model, with the minimum Membership Function (MF) or fuzzy rules significantly reducing the complexity;
- Simple and explicit if-then fuzzy rules are used to represent the mapping between inputs and outputs and the ANFIS structure is easy to understand and implement;
- Model performance can be flexibly tuned as the number of MFs and training iterations can be altered easily.
- Rapid learning capacity, adaptation capability, and ability to model non-linearity.

The subsequent sections include the I-V and RF characterization of GaN HEMTs, preliminaries associated with ANFIS, development of an ANFIS-based model for GaN HEMTs, validation of the proposed model and techniques, and the integration of the proposed model into a CAD environment for circuit analysis and simulation.

II. METHODOLOGY

A. DEVICE LAYOUT AND CHARACTERIZATION

The typical structure of RF/microwave GaN-on-SiC HEMT is shown in Fig. 1. SiC is a preferred material for substrate and is used to reduce substrate loss and keep the device cool. Due to the presence of a strong polarization field across the AlGaN / GaN hetero-interface, a Two-Dimensional Electron Gas (2DEG) channel with high sheet carrier density of 10^{13} cm^{-2} is achieved without any doping. The surface states act as electron traps in the access region between metal contacts. Proper passivation is required to avoid leaking/trapping electrons from the gate metal plate under the influence of a large electric field for high-power operation. The field plate reshapes the electric field distribution in the channel and reduces its peak value on the drain side of the gate edge. As

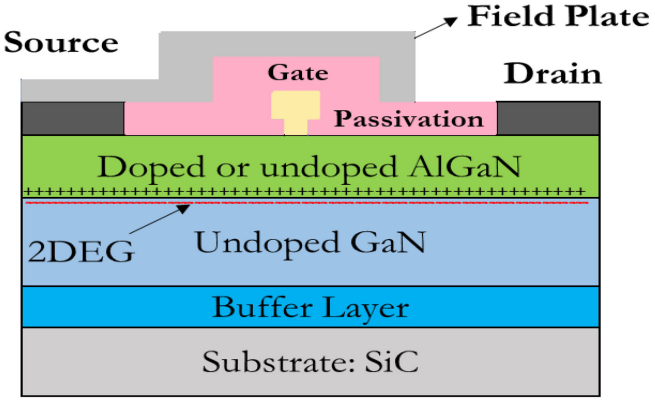

FIGURE 1. Typical structure of AlGaN/GaN HEMT.

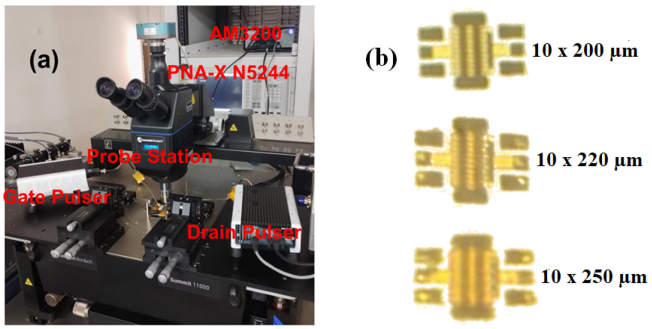

FIGURE 2. (a) Measurement set-up, and (b) layout of $10 \times 200\,\mu$m, $10 \times 220\,\mu$m and $10 \times 250\,\mu$m GaN HEMTs devices.

a result, the high-field trapping effect is significantly reduced and the breakdown voltage rises. A detailed discussion on the physics of GaN HEMT device is provided in [43].

The measurement set-up shown in Fig. 2(a) includes a Performance Network Analyzer (PNA), probe station, and DC/pulsed power supplies. The transistor is biased at the gate and the drain terminals through the power supplies using external bias tees, with the source terminal grounded. GaN-on-SiC devices of geometries $10 \times 200\,\mu$m, $10 \times 220\ \mu$m and $10 \times 250\ \mu$m, shown in Fig. 2(b) were provided by the Space Application Centre, Indian Space Research Organization (SAC-ISRO). DC I-V and CW S-parameters characterization of devices $10 \times 200\,\mu$m, $10 \times 220\ \mu$m are done under the conditions $-7\ \text{V} \leq V_{GS} \leq 0\ \text{V}$ and $0\ \text{V} \leq V_{DS} \leq 30\ \text{V}$ for a broad frequency range of 0.5 GHz-43.5 GHz using an AMCAD AM3200 system and Keysight PNA-X N5244A, respectively, at 25°C. Steady-state DC measurement of current with varying biases forms the basis for the understanding of the electrostatics of GaN devices. The PNA-X is calibrated using the Through-Reflect-Line (TRL) technique for S-parameter measurements of all three devices for different sets of V_{DS} with a step size of 5 V as it is a more appropriate technique for frequencies above 6 GHz and can be used for on-wafer calibrations as well. For $10 \times 250\ \mu$m device, the range of V_{GS} has been extended to 1.4 V.

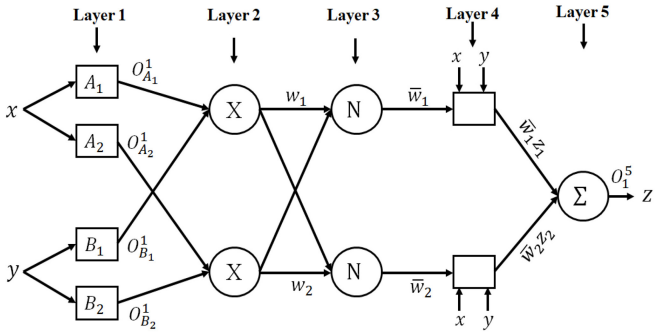

FIGURE 3. Typical architecture of the ANFIS.

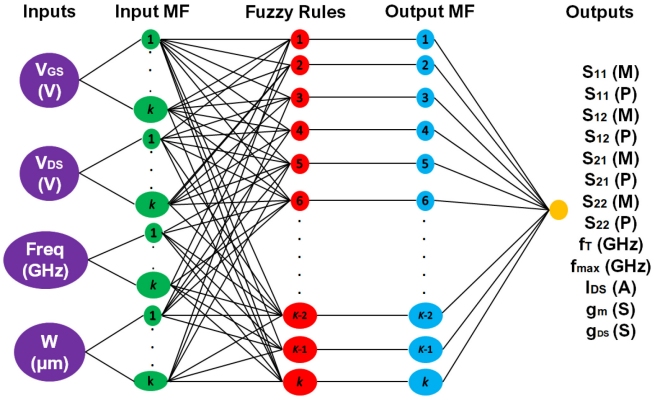

FIGURE 4. Proposed neuro-fuzzy based behavioral model of GaN HEMTs; (k represents the number of fuzzy rules).

B. BASIC PRINCIPLES OF ADAPTIVE NEURO FUZZY INFERENCE SYSTEM

In general, ANFIS is a multi-layer feed-forward neural network that, combined with supervised learning for the implementation of fuzzy decision rules, reveals the decision criteria based on the Takagi-Sugeno inference system [41], [42]. A basic architecture of ANFIS with two inputs, x and y, and one response z is shown in Fig. 3. For the given architecture, the rule base contains the following fuzzy if-then rules based on Takagi and Sugeno:

$$\begin{aligned} &\text{Rule 1 : If } x \text{ is } A_1 \text{ and } y \text{ is } B_1 \\ &\text{then } z_1 = p_1 x + q_1 y + r_1 \\ &\text{Rule 2 : If } x \text{ is } A_2 \text{ and } y \text{ is } B_2 \\ &\text{then } z_2 = p_2 x + q_2 y + r_2 \end{aligned} \tag{1}$$

where x and y are inputs to node i, A_i and B_i are linguistic labels associated with this node, z_i is the response, and (p_i, q_i, r_i) are the consequent parameters obtained during the training course. An ANFIS architecture consists of five stages and performs the respective functions at each stage - Fuzzification, Inference, Normalization, Accumulation, and Response. The various stages of ANFIS are described below:

Layer 1: Every node in the first layer implements fuzzy decision rules set up by the n MFs, such as $O^1_{A_i} = \mu_{A_i}(x)$, where x is the input of node i, O_{A_i} represents the linguistic labels of MF, $O^1_{A_i}$ represents the degree to which x satisfies A_i by using the MF ($\mu_{A_i}(x)$).

Layer 2: Each node in this layer evaluates the firing strength of every rule via multiplication. Subsequently, the relationships between linguistic labels are determined.

$$O^2_i = w_i = \mu_{A_i}(x).\mu_{B_i}(y) \tag{2}$$

Layer 3: In this layer, every conjunctive MF is normalized.

$$O^3_i = \tilde{w}_i = \frac{w_i}{w_1 + w_2} \quad i = 1, 2. \tag{3}$$

Layer 4: Here the parameters, specifically called consequent parameters (p_i, q_i, r_i), are determined with every node evaluating the i^{th} rule and contributing towards the overall response.

$$O^4_i = \tilde{w}_i f_i = \tilde{w}_i(p_i.x + q_i.y + r_i) \tag{4}$$

Layer 5: Eventually, the total response of the function, which is the sum of all fuzzy rules, is computed by a single node.

$$O^5_i = z_i = \sum_i \tilde{w}_i f_i = \frac{\sum_i w_i f_i}{\sum_i w_i} \tag{5}$$

The proposed ANFIS-based GaN HEMT models are fuzzy logic models with rules developed during training or learning. The training process completely relies on measured characteristics. The proposed technique draws a FIS whose MF parameters are extracted from training examples. In general, two commonly used FIS are Sugeno and Mamdani. The Sugeno-based FIS system is employed in this study since it is comparatively more computationally efficient than the Mamdani system. The output membership functions of the Sugeno system can be either constant or linear, which is the main distinction between it and the Mamdani system. However, the Mamdani FIS's output membership functions can also be Gaussian, trapezoidal, or triangular. Mamdani type significantly depends on expert knowledge, but the Sugeno type is trained using actual data.

C. INPUT SELECTION AND DEVELOPMENT OF INITIAL FUZZY INFERENCE SYSTEM FOR GAN HEMTS

The work proposes two different models: the first one models the I-V characteristics and its associated parameters such as trans-conductance (g_m) and output conductance (g_{ds}), whereas the second model develops the RF characteristics (S-parameters) and performance parameters (f_T and f_{max}). An ANFIS architecture of the GaN HEMT models including I-V and RF characteristics is shown in Fig. 4. The inputs to the models are V_{GS} (V), V_{DS} (V), frequency (GHz), and effective width $W(\mu m)$ = NF x W_{ug} (μm) where NF, W_{ug} (μm) and $W(\mu m)$ denotes num of fingers, unity gate width and effective gate width respectively.

The primary step that must be initiated in fuzzy modeling is the input selection process. This step identifies an input subset, within the designer input set, that has the potential of producing the best response. The significance of executing

this exercise is to discard the irrelevant inputs that do not affect models and those whose dependency is on other input parameters. This makes the proposed models more transparent and concise, simultaneously reducing model development computational time. The input selection method assumes that after one epoch of training, the ANFIS-based proposed transistor model with the lowest cost function (mean square error (MSE)) defined in [24], [31], [38] has a higher potential to achieve the best MSE after further epochs in the training stage. This may not be precisely true, but heuristically reasonable.

The framework for developing ANFIS-based behavioral models of GaN HEMTs is initiated by building an initial FIS for each input configuration using the SC algorithm. The expression in (6) yields the number of fuzzy models M.

$$M = \sum_{i=1}^{N} C_i^n \tag{6}$$

where n is the num of candidate inputs, and C_i^n are combinations of n inputs selected i at a time. After obtaining various initial FIS models, the models are trained with a single round of LSE using one epoch of the ANFIS algorithm. Subsequently, the model providing the best performance (lowest MSE) is chosen for the complete training using ANFIS.

D. SUBTRACTIVE CLUSTERING ALGORITHM ADOPTED FOR THE DEVELOPMENT OF THE PROPOSED TRANSISTOR MODEL

Using the traditional Takagi Sugeno model can cause a few problems for non-linear device modeling. The models' inability to reason when the input dimension is too huge is the main cause. The second issue is that rule numbers will expand exponentially as the dimensional complexity of the input space increases, resulting in a "rule disaster." Finding a suitable structure thus becomes crucial, and as a result, the clustering technique [44], [45] has been used as a precautionary measure to tackle a couple of issues in this research work. SC is used for developing proposed models as its estimation is directly proportional to the number of data points and independent of the dimension of the problem under consideration. This approach leads to simpler and faster FIS microwave power transistor models with only a few fuzzy rules, even for a considerable number of inputs. Full steps to this algorithm can be found in [46], however, some key points governing this algorithm are listed below:

1. The density measure for each cluster center of an input x represented by the dataset $(x_1, x_2, \ldots.., x_n)$ is calculated by

$$D_i = \sum_{j=1}^{n} exp\Big(-\alpha(||x_i - x_j||^2)\Big) \quad where \quad \alpha = 4/r_a^2, r_a \geq 0 \tag{7}$$

Here, r_a is a positive constant. The estimation of the potential for a data point is a function of its distances to all other data points. A data point with its associated neighbor data points will exhibit a relatively higher potential value. The proximity boundary is defined by the effective radius r_a; data points outside of this limit will have very little effect on the potential.

2. The dataset with the largest density is selected as the first cluster center x_1^*. The density measure for each data point is re-evaluated as:

$$D_i = D_i - D_1^* exp\Big(-\beta(||x_i - x_1^*||^2)\Big) \quad where \quad \beta = 4/r_b^2, r_b \geq 0 \tag{8}$$

Here, r_b is a positive constant. At this stage, we subtracted an amount of potential from each data point as a function of its distance from the first cluster center. This will greatly reduce the potential of data points near the first cluster center and hence unlikely to be selected as the next cluster center. Therefore, r_b is the effective radius of the data points in the neighborhood that will have reasonable reductions in potential.

3. Subsequently, the next center of clusters x_z^* is determined and an iterative procedure is followed according to (8), where r_b is a positive constant representing the radius of the neighborhood for which significant potential reduction will occur. After revising the density function, the next cluster center is selected as the point having the greatest potential value. This process is repeated to generate the cluster centers until the maximum potential value in the current iteration is equal to or less than the threshold.

$$D_i = D_i - D_z^* exp\Big(-\beta(||x_i - x_z^*||^2)\Big) \quad until \quad D_k^* < 0.2D_1^* \tag{9}$$

4. To avoid closely spaced cluster centers, it is better to opt for $r_b = 1.25 * r_a$, where $0.1 \leq r_a \leq 0.5$. After evaluating all the cluster centers, each one is translated into a fuzzy system. Considering a Sugeno-type FIS, fuzzy rules in general are:

$$\text{Rule } i = \text{If } X_1 \text{ is } A_{i1} \text{ and } X_2 \text{ is } A_{i2} \text{ and}, \ldots \quad then \quad f_i = p_{i0} + p_{i1}X_1 + p_{i2}X_2 + \cdots\cdots$$

where f_i is the output variable and p_{i0}, p_{i1}, p_{i2} are optimized consequent parameters obtained after model training. The membership degree is represented by the expression (10)

$$\mu_i = exp\Big(-\alpha||x - x_i^*||^2\Big) \tag{10}$$

This approach generates the number of fuzzy rules of the Sugeno-type FIS transistor model and the antecedent MFs. The consequent parameters $(p_{10}, \ldots, p_{ij})$ of each rule of a Sugeno-Type FIS are determined using the LSE algorithm during ANFIS training of the models. Membership functions graphically represent fuzzy sets. This work makes use of the Gaussian membership function $M_{ij}X(j)$ with the i^{th} rule for

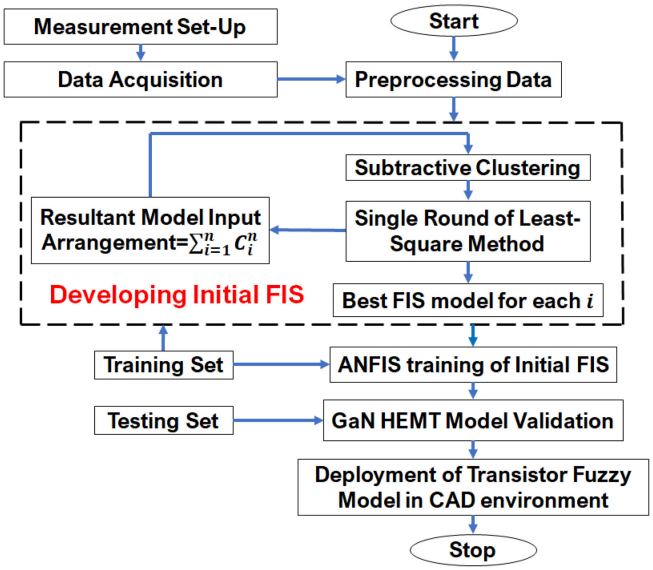

FIGURE 5. Flowchart for the development of ANFIS-based GaN HEMTs models.

each input variable $X(j)$ defined and expressed in (11), where σ and x_{ij}^{*} denotes standard deviation and mean respectively.

$$M_{ij}(X_j) = exp\left[-\frac{1}{2}\left(||x_i - x_{ij}^{*}||/\sigma_{ij}^{2}\right)\right]$$
$$where \qquad \sigma_{ij}^{2} = \frac{1}{2\alpha} \tag{11}$$

The flowchart of the complete modeling exercise is shown in Fig. 5. The radius of the clusters will be used as the basis of the cluster formation. To obtain the optimal number of clusters for the initial fuzzy inference system (FIS) of the proposed GaN HEMT models, a radius range of 0.1 to 0.5 has been selected. The initial FIS is then fed to the ANFIS for refining the FIS so that it will tune the supervised learning iteratively with more detailed rules generated. Each cluster center represents a fuzzy if-then rule. The n^{th} column of c^{th} cluster center is assumed to be the mean value of the associated Gaussian membership function defined for c^{th} fuzzy set of n^{th} input variable.

E. ANFIS MODEL TRAINING AND FINAL FIS GaN HEMT MODEL

GaN HEMTs FIS models are further trained using a hybrid learning algorithm (neural network adaptive learning) using complete measured I-V, S-parameters, and RF performance characteristics of two devices $10 \times 200\,\mu$m and $10 \times 250\,\mu$m. A couple of necessary training steps are - structure learning which allows one to determine the appropriate structure of the network, i.e., the best partitioning of the input space (number of membership functions for 4 inputs, number of rules), and parametric learning is carried out to adjust the membership functions and consequent parameters. The hybrid algorithm consists of a forward stage and a backward stage for each training iteration and combines a back-propagation algorithm and least squares method. During the forward process, node outputs go forward till layer 4 and the consequent parameters are identified by the LSE by keeping the antecedent parameters constant. During the backward process, the errors are propagated as feedback, and subsequently, the GD algorithm updates the premise (antecedent) parameters. Table 1 summarizes the activities in each pass. It is imperative to mention that the consequent parameters are fixed during the backward process. The model has set output MFs to be constant.

TABLE 1. Summary of hybrid learning procedure for ANFIS.

	Forward Pass	Backward Pass
Antecedent Parameters	Fixed	GD
Consequent Parameters	LSE	Fixed
Signals	Node Output	Error

After the completion of training, the next step is to affirm the accuracy and generalization capabilities of the FIS models and subsequently opt for the best final FIS models for GaN HEMTs. MSE, a well-known performance indicator has been employed as the criteria to select the best FIS model. In choosing the best FIS models for I-V, RF characteristics, and S-parameters of GaN HEMTs, an important factor of highest consideration was that the final FIS models must employ the least number of rules and inputs to make it highly interpretable and computationally efficient. SC used in the input selection process is obtained using the value r_a=0.5. However, other values of r_a (0.1,0.3,0.5) have also been tested to build initial ANFIS-based training utilizing the best inputs. ANFIS and SC algorithms are implemented in MATLAB. It is apparent from Fig. 6 that the smallest r_a produces more rules for GaN HEMTs Sugeno model. The opposite holds for the largest value for r_a.

The best FIS model for GaN HEMTs has been chosen against the cluster radius r_a=0.5 which yields fewer rules and the smallest error simultaneously. The total epoch that was needed to train the model was 50. However, it was observed that after 20 epochs error value became constant. For a better understanding, the fuzzy activation rules for S-parameters and the degree of membership for I-V characteristics are shown in Figs. 7 and 8, respectively. 16 and 31 and 12 fuzzy if-then rules are obtained from the best FIS model to model I-V, S-parameters, and RF performance (f_T and f_{max}) characteristics respectively with accuracy. Fig. 7 reveals the different sets of Gaussian coordinates [x_{ij}^{*}, σ] used to form clusters or fuzzy rules. Table 2 and Table 3 provides the explicit mathematical representation for modeling $|S_{12}|$ and I_{DS} respectively. It can be seen from the tables that the various inputs are represented in the form of cluster centers [x_{ij}^{*}, σ] and corresponding output variable is expressed in linear equation with optimized set of consequent parameters (p_{i0},p_{i1},p_{i2},p_{i3}, p_{i4}) which in turn aids in framing set of fuzzy rules. The trained model is obtained by setting Gaussian MF at the inputs and linear MF at the output node.

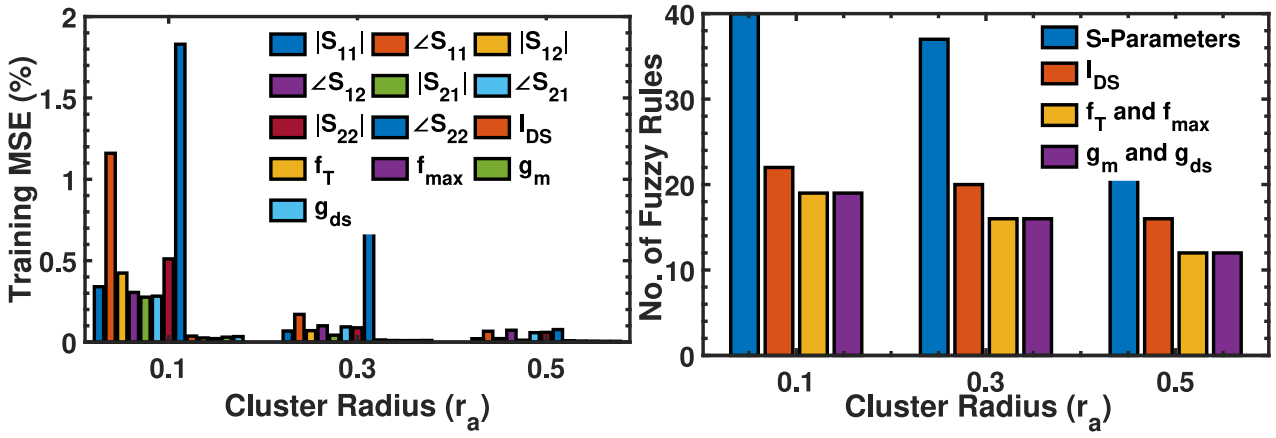

(a) (b)

FIGURE 6. Criteria for selection of best FIS model: Plotting (a) train set error of GaN HEMT model, and (b) num of Fuzzy rules against cluster radius r_a.

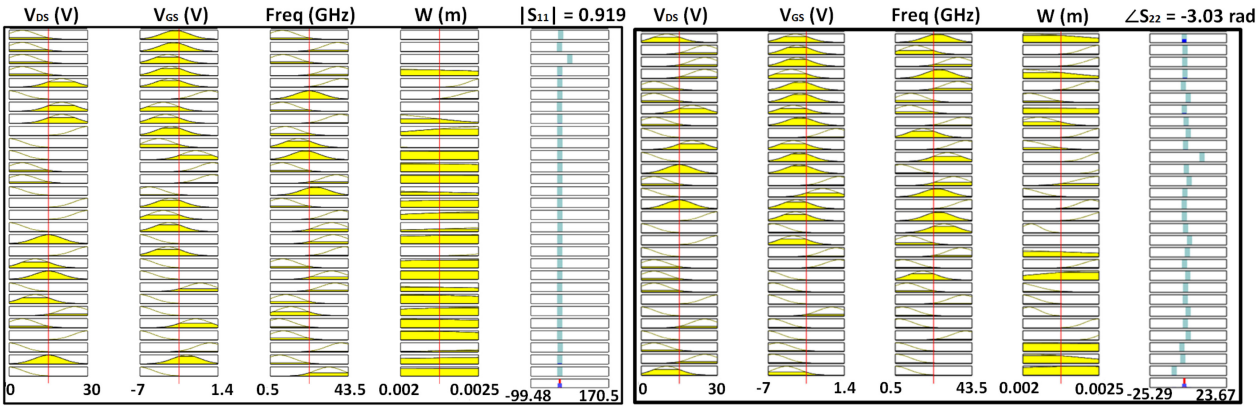

(a) (b)

FIGURE 7. Fuzzy activation rules obtained from final FIS model in verbose format for (a) $|S_{11}|$, and (b) $\angle S_{22}$ (radian) for r_a=0.5.

TABLE 2. Optimized gaussian clusters centers and consequent parameters for modeling $|S_{12}|$.

Inputs/ Rules	V_{DS} Cluster $[x^*_{ij}, \sigma]$	V_{GS} Cluster $[x^*_{ij}, \sigma]$	Frequency (f) Cluster $[x^*_{ij}, \sigma]$	W (m) Cluster $[x^*_{ij}, \sigma]$	Output Equation $\lvert S_{12}\rvert = (p_{i0} + p_{i1} * V_{DS} + p_{i2} * V_{GS} + p_{i3} * f + p_{i4} * W)$
Rule 1	[5.3014, 9.999]	[1.484, -3.6]	[7.601,24.799]	[9.343e-5, 0.00249]	-0.00124 + 0.0223 * V_{DS} - 0.0068 * V_{GS} + 0.0029 * f + 1.2 * W
Rule 6	[5.303, 4.999]	[1.485, -3.398]	[7.602,9.099]	[7.5102e-5, 0.0025]	-0.01012 + 0.0602 * V_{DS} - 0.0144 * V_{GS} + 0.035 * f + 1.401 * W
Rule 12	[5.303, -1.365e-6]	[1.484, -3.25]	[7.601, 36]	[7.28e-5, 0.00199]	-0.00044 + 0.02289 * V_{DS} - 0.000328 * V_{GS} + 0.002 * f + W
Rule 16	[5.303, -7.593e-5]	[1.485, 0.5005]	[7.601, 34.7]	[9.985e-5, 0.00249]	0.0986 + 0.0228 * V_{DS} - 0.01368 * V_{GS} + 0.0042 * f + 1.71 * W
Rule 21	[5.303, -4.516e-5]	[1.484, -5.999]	[7.601, 31.5]	[9.18e-5, 0.00249]	0.00064 - 0.0101 * V_{DS} - 0.00152 * V_{GS} + 0.0022 * f + 0.91 * W
Rule 28	[5.303, 5]	[1.484, 0.799]	[7.601, 36.399]	[8.387e-5, 0.0025]	0.02705 + 0.044 * V_{DS} + 0.0243 * V_{GS} - 0.00142 * f - 0.571 * W
Rule 31	[5.303, 8.95e-6]	[1.484, -6.5]	[7.601, 32.5]	[6.055e-5, 0.00199]	-0.0004 + 0.0107 * V_{DS} + 0.0022 * V_{GS} - 0.0018 * f + 0.89 * W

TABLE 3. Optimized gaussian clusters centers and consequent parameters for modeling I_{DS}.

Inputs/ Rules	V_{DS} Cluster $[x^*_{ij}, \sigma]$	V_{GS} Cluster $[x^*_{ij}, \sigma]$	W (m) Cluster $[x^*_{ij}, \sigma]$	Output Equation $I_{DS} = (p_{i0} + p_{i1} * V_{DS} + p_{i2} * V_{GS} + p_{i3} * W)$
Rule 1	[5.303, 2]	[1.414, -3.7]	[8.838e-5, 0.0025]	-0.02878 - 0.363 * V_{DS} - 0.0039 * V_{GS} - 1.59 * W
Rule 2	[5.303, 5]	[1.414, -4.24]	[8.838e-5, 0.002]	0.05092 - 1.51 * V_{DS} - 0.0147 * V_{GS} - 7.35 * W
Rule 5	[5.303, 25]	[1.414, 4.49]	[8.838e-5, 0.002]	-0.1187 - 3.704 * V_{DS} + 0.01715 * V_{GS} + 8.57 * W
Rule 8	[5.303, 2]	[1.414, -1]	[8.838e-5, 0.0025]	0.6742 - 1.236 * V_{DS} - 0.003686 * V_{GS} - 1.47 * W
Rule 11	[5.303, 1]	[1.414, -1.5]	[8.838e-5, 0.002]	1.054 - 2.209 * V_{DS} - 0.004663 * V_{GS} - 2.33 * W
Rule 13	[5.303, 20]	[1.414, -6.99]	[8.838e-5, 0.0025]	0.00934 + 0.2895 * V_{DS} + 0.00468 * V_{GS} + 1.87 * W
Rule 14	[5.303, 15]	[1.414, -2.99]	[8.838e-5, 0.002]	0.07086 + 0.5245 * V_{DS} + 0.00648 * V_{GS} + 3.24 * W
Rule 15	[5.303, 20]	[1.414, -7]	[8.838e-5, 0.002]	0.02487 + 0.2707 * V_{DS} + 0.00295 * V_{GS} + 1.47 * W
Rule 16	[5.303, 10]	[1.414, -2]	[8.838e-5, 0.0025]	0.2937 - 0.2904 * V_{DS} - 0.01068 * V_{GS} - 4.27 * W

ANFIS-based modeling over machine learning techniques is demonstrated to model I-V and S-parameter features with clear mathematical representation, akin to a relative glass box approach. In terms of AI, a set of rules is expressed using a logical relationship between input and output variables using logical connectives such as AND ($\wedge$), OR ($\vee$), Implication

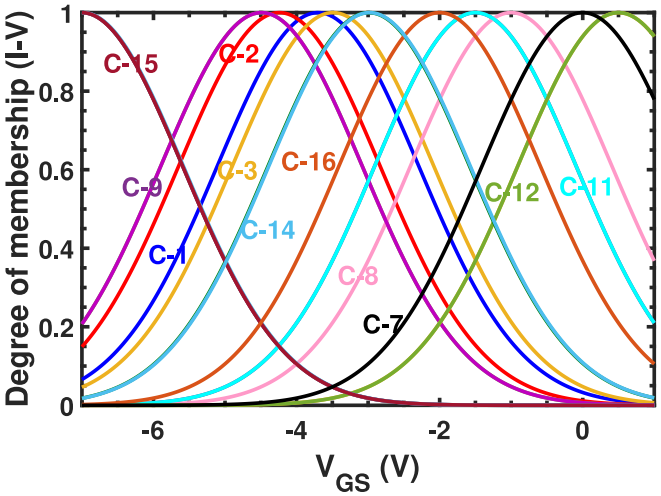

FIGURE 8. MF of I_{DS} (A) against V_{GS} (Volts) for r_a = 0.5. C-1 to C-16 represent no. of clusters formed to model I-V characteristics. The horizontal axis represents the universe of discourse whereas the vertical axis specifies the degree of membership in the interval [0,1].

RULE 1: If V_{DS} == Cluster1 of V_{DS} ∧ V_{GS} == Cluster1 of V_{GS} ∧ W == Cluster1 of W ⇒ f_T = Cluster1 of f_T

RULE 2: If V_{DS} == Cluster2 of V_{DS} ∧ V_{GS} == Cluster2 of V_{GS} ∧ W == Cluster2 of W ⇒ f_T = Cluster2 of f_T

RULE 3: If V_{DS} == Cluster3 of V_{DS} ∧ V_{GS} == Cluster3 of V_{GS} ∧ W == Cluster3 of W ⇒ f_T = Cluster3 of f_T

.
.

RULE 11: If V_{DS} == Cluster11 of V_{DS} ∧ V_{GS} == Cluster11 of V_{GS} ∧ W == Cluster11 of W ⇒ f_T = Cluster11 of f_T

RULE 12: If V_{DS} == Cluster12 of V_{DS} ∧ V_{GS} == Cluster12 of V_{GS} ∧ W == Cluster12 of W ⇒ f_T = Cluster12 of f_T

FIGURE 9. Fuzzy activation rules for f_T in symbolic format.

($\Longrightarrow$), Biconditional ($\longleftrightarrow$) and quantifiers as shown in Fig. 9.

F. MODEL VALIDATION: RESULTS AND DISCUSSIONS

The best-trained FIS models for I-V characteristics, S-parameters, and RF characteristics of GaN HEMTs are finalized for r_a=0.5. Eventually, the last step is to establish the validation of accuracy and generalization capabilities of the best FIS model obtained. The present section validates the effectiveness, reliability, and prediction ability of the proposed GaN HEMTs FIS models on three sets of devices. The first testing will be done on a transistor of dimension $10 \times 220\,\mu$m (not involved in the training phase) for a range of applied bias and frequency to establish the interpolation ability of the ANFIS technique for device modeling.

In the first exercise, it can be seen that the proposed technique has accurately modeled the I-V characteristics and associated effects like self-heating for multiple values of V_{DS} and V_{GS}, as shown in Figs. 10(a) and 10(b) respectively. The transconductance g_m increases monotonically with increasing V_{GS} around the threshold voltage (−3.75 V) as shown in Fig. 10(c) and approaches a constant value as electron velocity saturates at high electric fields along the channel. g_m approaches a maximum value of 0.62 S. Similarly, g_{ds} increases with an increase in V_{GS} and attains a maximum value of 0.91 S in the ohmic region as shown in Fig. 10(d). The modeled characteristics closely follow measured g_m and g_{ds} characteristics as demonstrated in Figs. 10(c) and 10(d) with g_m forming a characteristic bell shape.

Moreover, RF performance characteristics f_T and f_{max} are first extracted using the expression in [22], [38], and the extracted values of two devices are subsequently used to build the FIS models. It is to be noted that f_T and f_{max} are functions of g_m and follow the same trend due their linear dependency on the transconductance. A good agreement obtained between the measured and the modeled RF-performance parameters as shown in Fig. 10(e) and Fig. 10(f) for multiple bias conditions demonstrates validation of f_{max} and f_T following the same trend as that of g_m. The small-signal performance of the test device is validated by comparing the measured S-parameters with modeled characteristics in Fig. 11. It is well established that the proposed ANFIS-based approach can accurately simulate the S-parameters in both the linear and saturation regimes. Moreover, it can also predict the kink effect in S_{22} as shown in Fig. 11(d) for V_{DS}= 20 V, V_{GS}= −2.5 V, which occurs in large periphery transistors and relies on the frequency dependence of the device output impedance.

F.1. EXTRAPOLATION POTENTIAL OF THE PROPOSED ANFIS-BASED GAN HEMTS MODELS

This section investigates the extrapolation potential and scalability of the proposed ANFIS-based modeling technique. To manifest these features, the proposed model is validated using a couple of devices with geometries $2 \times 200\,\mu$m and $4 \times 100\,\mu$m based on I-V and S-parameter characteristics. The fabricated AlGaN/GaN HEMT testing device, not shown here due to manufacturer's policy, of geometries $2 \times 200\,\mu$m and $4 \times 100\,\mu$m is shown in Fig. 12. These devices, grown on SiC substrate, are fabricated by the Defense Research Development Organization (DRDO), an enterprise of the Ministry of Defense, Govt. of India). The characterization setup includes a Microwave Network Analyzer, probe station, and DC power supplies. The biasing to the device is provided at the gate and the drain terminals, with the source terminal being grounded, through DC power supplies using bias Tees internal to the network analyzer. The characterization is done under the small-signal conditions for $-7\ \text{V} \le V_{GS} \le 0$ V, $0\ \text{V} \le V_{DS} \le 10$ V for a frequency range of 1-18 GHz. The S-parameters are recorded in terms of magnitude and phase of two-port S-parameters for the provided multi-biasing and frequency range.

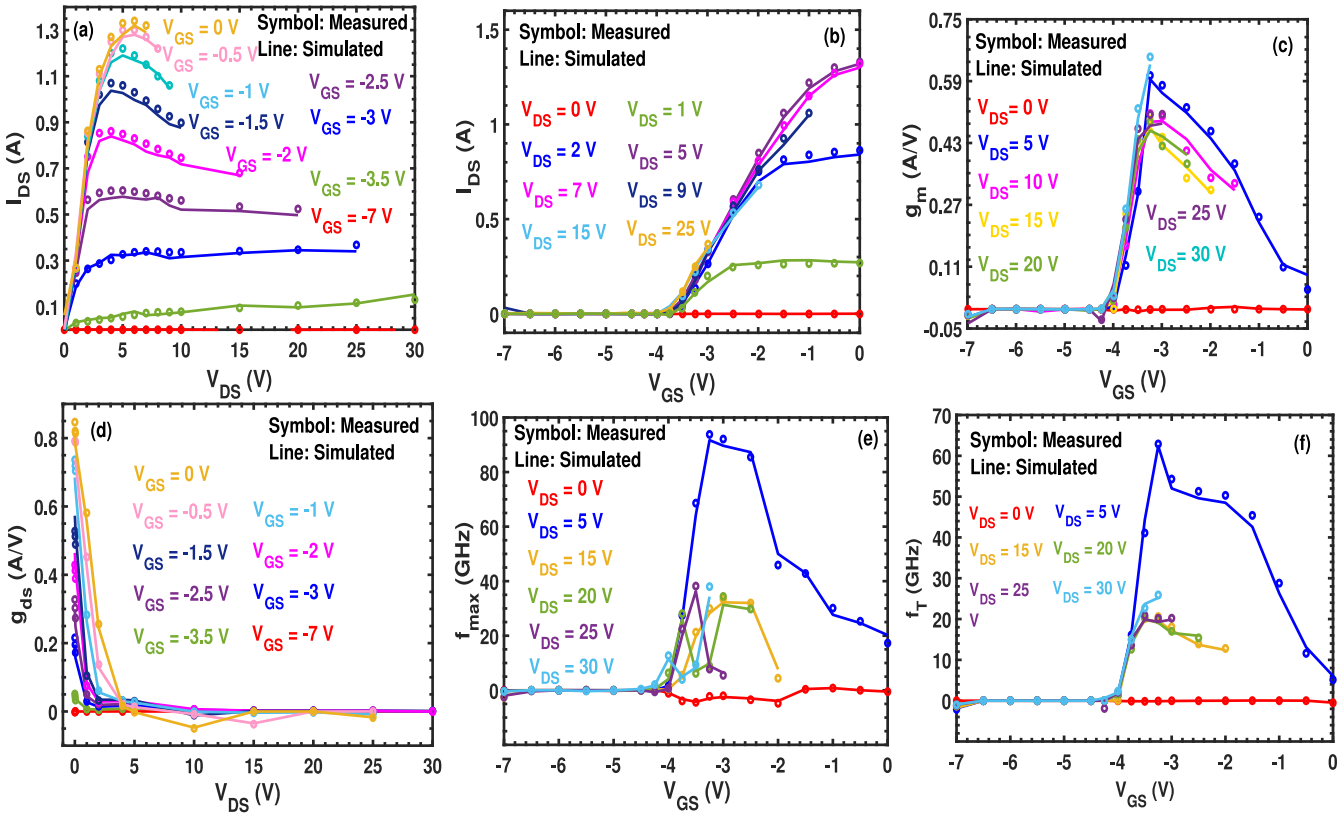

FIGURE 10. Comparison between the measured data and the modeled characteristics on test device 10 × 220 μm (a) I_{DS} - V_{DS}, (b) I_{DS} - V_{GS}, (c) g_m - V_{GS}, (d)g_{ds} - V_{DS}, (e) f_{max} - V_{GS}, and (f) f_T - V_{GS} for different V_{GS} and V_{DS} respectively.

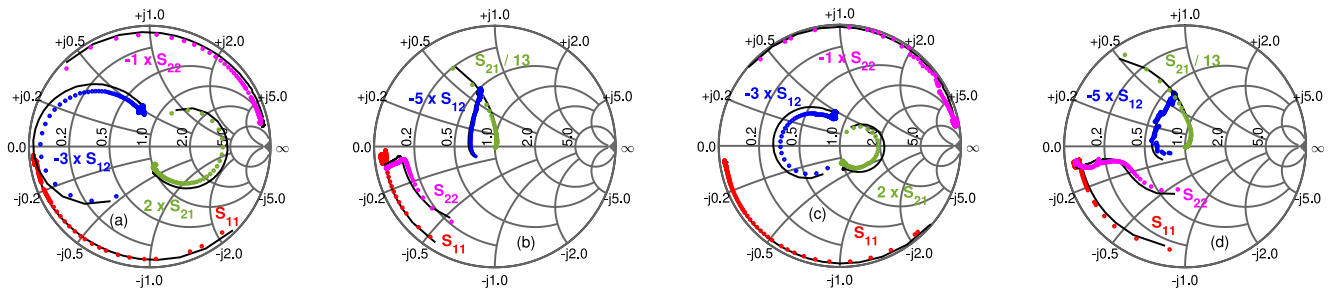

FIGURE 11. Comparison between the measured (line) data and the ANFIS based S-parameters GaN HEMTs (simulated) on test device 10 × 220 μm for multi-bias S-parameters covering a broad frequency range of 0.5-43.5 GHz - (a) V_{DS} = 5 V; V_{GS} = −4.5 V, (b) V_{DS} = 5 V; V_S = −2.5 V, (c) V_{DS} = 20 V; V_{GS} = −4.5 V, and (d) V_{DS} = 20 V; V_{GS} = −2.5 V.

The complete procedure for testing extrapolation ability over new sets of geometrical devices is briefly summarized in Fig. 13. Initially, the input set in terms of V_{GS}, V_{DS}, effective width W = 0.0004 m and frequency (in case of S-parameters) is provided to the final FIS GaN HEMTs models, and the modeled output for both the devices will remain same irrespective of the device of geometry 2 × 200 μm or 4 × 100 μm. This is a limitation that is inherent with the development of the proposed model where effective width is considered as an input instead of number of fingers (N) and unity gate width $W_{ug}(\mu m)$. To overcome such a problem, switch and case statements are utilized in our developed MATLAB program which picks measured i/p-o/p characteristics of a device under test at a time based on N and $W_{ug}(\mu m)$. This step easily differentiates two different geometrical devices with the same W. The inputs of the device under test (DUT) are fed to GaN HEMTs FIS model and the evaluated response is calculated. Optimization or tuning is needed to maximize accuracy and reduce error between the estimated and the measured response. However, all the inputs of FIS models are deliberately set to "not to tune" mode to ensure the width scalability of the proposed under the same set of values of the input variable. The evaluated output is compared with the measured output of the device. The cost function unit evaluates the deviation and pushes the algorithm towards optimization or tuning to

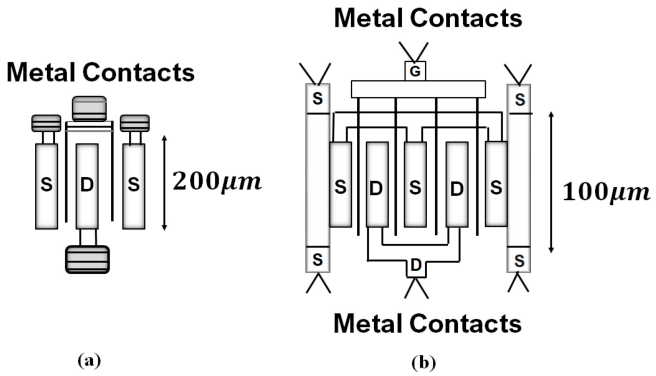

FIGURE 12. Layout of (a) 2 × 200 μm, and (b) 4 × 100 μm GaN HEMTs devices.

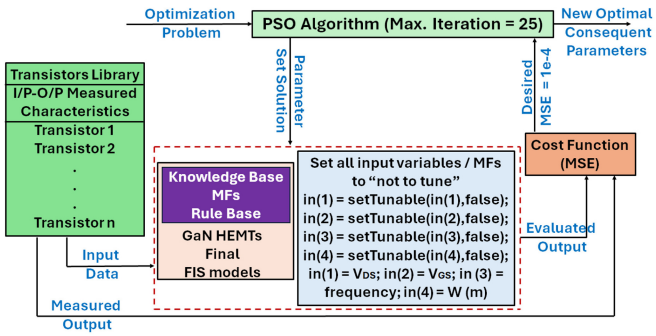

FIGURE 13. Tuning the proposed GaN HEMTs Final FIS models: Manifesting Extrapolation accuracy and scalability.

minimize the deviation between the estimated and the desired response. Particle Swarm Optimization (PSO) algorithm [45] is used for optimizing or tuning. The termination criteria of the optimization are set either to MSE = 1e-4 or the maximum iteration set to 25. After reaching the termination criteria, a new set of optimal consequent parameters $(p_{10}, \ldots, p_{ij})$ is obtained which best fits the measured and simulated characteristics. Similarly, the same procedure is used to evaluate the response of the second device under test and subsequently tune the modeled characteristics to achieve the best fit with the measured characteristics. On comparing, Table 2 with Table 5 and Table 3 with Table 4, it is apparent that MF coordinates $[x_{ij}^*, \sigma]$ of all input variables (antecedent parameters) remains same as that of GaN HEMT Final FIS models but new optimal output cluster (consequent parameters) equations are obtained for accurately modeling $|S_{12}|$ and I_{DS} of 2 × 200 μm and 4 × 100 μm devices. An excellent agreement between the measured and the simulated I-V characteristics and its associated parameters such as g_m, S-parameter characteristics can be validated using Fig. 14(a) - 14(f). This also proves the greater flexibility of the proposed algorithm and modeling approach which is used to achieve accuracy over the extrapolation range and ensure a width-scalable model.

It is an important observation that the kink effect is not being observed in the tested transistor as can be noticed in Fig. 14(e) and Fig. 14(f). The effect is entirely due to the intrinsic parameters of the device and the shape of the kink is affected by the extrinsic elements of the device. The intrinsic elements of the device small signal model determine the value of output impedance Z_{out} and S_{22} being strongly dependent on Z_{out} gets affected by change in intrinsic parameters of the device such as g_m, capacitances (C_{gd}, C_{ds}, C_{gs}). Kink becomes more noticeable with an increase in g_m and C_{gd} and an increase in C_{gs} shifts the kink. The tested transistors in this instance are small periphery transistors, and their g_m value is 0.095 S, which is around seven times less than the value of the huge periphery transistors that were utilized to develop the model. This explains why tested transistors do not exhibit the kink effect. In addition, the kink effect is more prominent with an increase in V_{GS} which is due to higher g_m as long as self-heating is not observed [47], [48].

F.2. COMPARATIVE DISCUSSION BETWEEN THE PROPOSED APPROACH AND THE ESTABLISHED APPROACH OF MODELING GaN HEMTS

This section provides an in-depth comparison based on the framework, architecture, parameters, and performance between the proposed method and existing modeling approaches for modeling GaN HEMTs, such as ML, empirical, and physics-based modeling approaches. First, a succinct and comprehensive comparison of the suggested ANFIS approach with existing ML techniques, including SVR and DT, for modeling microwave power transistors based on different parameters are given in Table 6. Unlike SVR and DT, ANN and ANFIS modeling approaches are parametric models. Parametric models already assume a mapping function and estimate the coefficients of the variable to be optimized where the information is stored such as weights and bias in the case of ANN or the coefficients of antecedent and consequent parameters in the case of the proposed approach. Hence, methods like ANN and ANFIS are quicker and simpler to learn from data. However, the ANFIS-based modeling approach is easy to interpret as it is very much transparent in establishing the mapping function in the form of equations and rules between both inputs and response sides that are understandable to humans as expressed in Tables 2, 3, 4 and 5 but ANN based GaN HEMTs models are not able to completely reveal the mapping function explicitly. With the proposed technique, the number of computational layers is fixed at 5, but with an ANN, the number of computational layers varies depending on how many hidden layers are set for the model's development. However, SVR AND DT are non-parametric machine learning algorithms. It indicates that aside from similar patterns that probably have comparable output variables, non-parametric machine learning algorithms do not make any significant assumptions regarding the nature of the mapping function. As a result, they can use the training data to learn any functional form. They can therefore best fit the data while retaining the capacity to generalize to previously unseen data. As such, they can fit a large number of functional forms

TABLE 4. Optimal consequent Parameters for modeling I-V characteristics of 2 × 200 μm and 4 × 100 μm.

Inputs/ Rules	V_{DS} Cluster $[x^*_{ij}, \sigma]$	V_{GS} Cluster $[x^*_{ij}, \sigma]$	W (m) Cluster $[x^*_{ij}, \sigma]$	Output Equation ($2 \times 200\,\mu$m) $I_{DS} = (p_{i0} + p_{i1} * V_{DS} + p_{i2} * V_{GS} + p_{i3} * W)$	Output Equation ($4 \times 100\,\mu$m) $\lvert S_{12}\rvert = (p_{i0} + p_{i1} * V_{DS} + p_{i2} * V_{GS} + p_{i3} * W)$
Rule 1	[5.303, 2]	[1.414, -3.7]	[8.838e-5, 0.0025]	0.474 + 0.486 * V_{DS} + 1.521 * V_{GS} + 1.343 * W	1.77 + 1.929 * V_{DS} - 0.0039 * V_{GS} + 0.337 * W
Rule 2	[5.303, 5]	[1.414, -4.24]	[8.838e-5, 0.002]	1.746 - 1.454 * V_{DS} + 1.871 * V_{GS} - 3.205 * W	-0.0015 - 1.335 * V_{DS} - 0.014 * V_{GS} - 6.983 * W
Rule 5	[5.303, 25]	[1.414, -4.49]	[8.838e-5, 0.002]	0.011 + 0.025 * V_{DS} + 0.743 * V_{GS} + 0.096 * W	0.182 + 0.489 * V_{DS} + 0.391 * V_{GS} + 0.605 * W
Rule 8	[5.303, 2]	[1.414, -1]	[8.838e-5, 0.0025]	1.475 - 0.904 * V_{DS} + 1.668 * V_{GS} - 1.371 * W	0.271 - 0.134 * V_{DS} + 1.204 * V_{GS} - 1.092 * W
Rule 11	[5.303, 1]	[1.414, -1.5]	[8.838e-5, 0.002]	0.189 - 2.174 * V_{DS} + 1.129 * V_{GS} + 1.738 * W	1.444 - 0.429 * V_{DS} + 0.124 * V_{GS} - 2.109 * W
Rule 13	[5.303, 20]	[1.414, -6.99]	[8.838e-5, 0.0025]	-0.00155 + 1.929 * V_{DS} + 1.306 * V_{GS} + 1.857 * W	1.619 + 0.609 * V_{DS} + 1.851 * V_{GS} + 0.073 * W
Rule 14	[5.303, 15]	[1.414, -2.99]	[8.838e-5, 0.002]	1.929 + 0.625 * V_{DS} - 0.0015 * V_{GS} + 0.315 * W	-0.0708 + 0.106 * V_{DS} + 0.032 * V_{GS} + 1.694 * W
Rule 15	[5.303, 20]	[1.414, -7]	[8.838e-5, 0.002]	0.295 + 1.777 * V_{DS} + 0.6408 * V_{GS} + 1.842 * W	0.888 + 1.389 * V_{DS} + 0.258 * V_{GS} + 1.4805 * W
Rule 16	[5.303, 10]	[1.414, -2]	[8.838e-5, 0.0025]	0.132 + 0.129 * V_{DS} + 0.0004 * V_{GS} + 0.462 * W	1.578 + 1.714 * V_{DS} + 0.375 * V_{GS} - 1.532 * W

TABLE 5. Optimal consequent Parameters for modeling $|S_{12}|$ of 2 × 200 μm and 4 × 100 μm.

Inputs/ Rules	V_{DS} Cluster $[x^*_{ij}, \sigma]$	V_{GS} Cluster $[x^*_{ij}, \sigma]$	Frequency (GHz) Cluster $[x^*_{ij}, \sigma]$	W (m) Cluster $[x^*_{ij}, \sigma]$	Output Equation ($2 \times 200\,\mu$m) $\lvert S_{12}\rvert = (p_{i0} + p_{i1} * V_{DS} + p_{i2} * V_{GS} + p_{i3} * f + p_{i4} * W)$	Output Equation ($4 \times 100\,\mu$m) $\lvert S_{12}\rvert = (p_{i0} + p_{i1} * V_{DS} + p_{i2} * V_{GS} + p_{i3} * f + p_{i4} * W)$
Rule 1	[5.3014, 9.999]	[1.484, -3.6]	[7.601,24.799]	[9.343e-5, 0.00249]	0.0225 + 0.055 * V_{DS} + 0.103 * V_{GS} + 0.213 * f + 1.136 * W	-0.00123 + 0.114 * V_{DS} - 0.0068 * V_{GS} + 0.1207 * f + 0.658 * W
Rule 6	[5.303, 4.999]	[1.485, -3.398]	[7.602,9.099]	[7.5102e-5, 0.0025]	0.289 + 0.283 * V_{DS} + 0.8008 * V_{GS} + 0.0777 * f + 1.179 * W	0.0202 + 0.273 * V_{DS} - 0.0144 * V_{GS} + 0.353 * f + 1.373 * W
Rule 12	[5.303, -1.365e-6]	[1.484, -3.25]	[7.601,36]	[7.28e-5, 0.00199]	0.0191 + 0.0233 * V_{DS} + 0.234 * V_{GS} + 0.054 * f + 0.9206 * W	0.1724 + 0.453 * V_{DS} + 0.0107 * V_{GS} + 0.002003 * f + 0.9311 * W
Rule 16	[5.303, -7.593e-5]	[1.485, 0.5005]	[7.601,34.7]	[9.985e-5, 0.00249]	0.639 + 0.192 * V_{DS} + 0.129 * V_{GS} + 0.215 * f + 0.793 * W	0.256 + 0.368 * V_{DS} + 0.304 * V_{GS} + 0.3902 * f + 1.577 * W
Rule 21	[5.303, -4.516e-5]	[1.484, -5.999]	[7.601,31.5]	[9.18e-5, 0.00249]	0.146 + 0.0043 * V_{DS} + 0.849 * V_{GS} + 0.196 * f + 0.725 * W	0.651 + 0.831 * V_{DS} - 0.00152 * V_{GS} + 0.214 * f + 0.673 * W
Rule 28	[5.303, 5]	[1.484, 0.799]	[7.601,36.399]	[8.387e-5, 0.0025]	0.548 + 0.236 * V_{DS} + 0.607 * V_{GS} + 0.172 * f - 0.571 * W	0.3202 + 0.0719 * V_{DS} + 0.196 * V_{GS} + 0.01055 * f - 0.00791 * W
Rule 31	[5.303, 8.95e-6]	[1.484, -6.5]	[7.601,32.5]	[6.055e-5, 0.00199]	0.3265 + 0.1709 * V_{DS} + 0.0223 * V_{GS} + 0.219 * f + 0.717 * W	0.00349 + 0.0147 * V_{DS} + 0.376 * V_{GS} + 0.00569 * f + 0.8132 * W

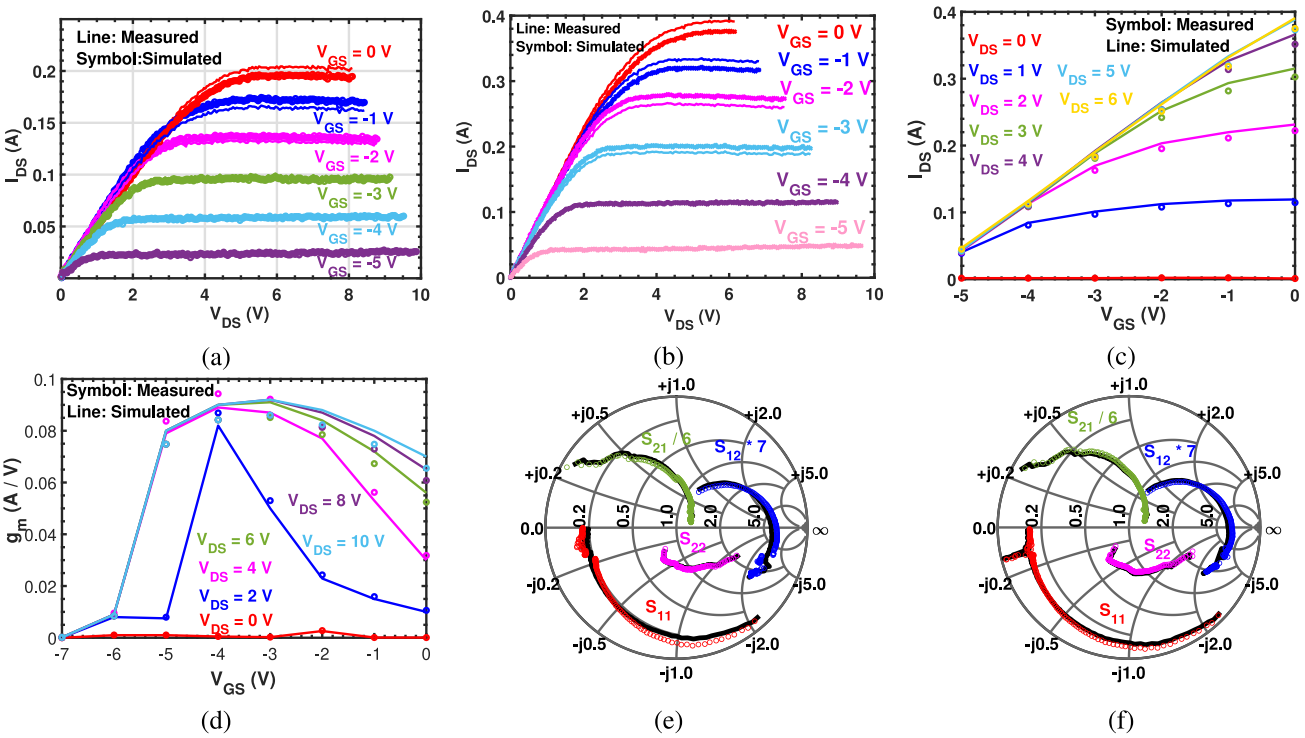

FIGURE 14. Validation of the extrapolation ability of the proposed ANFIS model-Comparison between the measured and the simulated characteristics: (a) I_{DS}-V_{DS} (2 × 200 μm), (b) I_{DS}-V_{DS} (4 × 100 μm), (c) I_{DS}-V_{GS} (4 × 100 μm), (d) g_m-V_{GS} (4 × 100 μm), (e) reflection and transmission S-parameters at V_{GS}= −2 V; V_{DS}= 8 V (2 × 200 μm), and (f) reflection and transmission S-parameters at V_{GS}= −2 V; V_{DS}= 8 V (4 × 100 μm).

TABLE 6. Comparison of parameters between the proposed ANFIS method and various ML-based modeling.

Parameters	Proposed ANFIS Method	ANN Method [24]-[25],[27]-[29]	SVR [30]-[33]	Decision Tree (DT) [24][34]
No. of layers	5	Size depends on no. of hidden layers	Optimal Hyperplane	Tree branches
Structures (I-V)	[3 16 16 16 16 1]	[3 10 10 3] (Hidden layer = 2)	Kernel	Tree Structure Branches
Structures (RF)	[4 32 32 32 1]	[4 25 25 10] (Hidden Layer = 2)	Kernel	Tree Branches
Learning Algorithm	Hybrid Method [42]	Levenberg-Marquardt, GD, GA	Sequential Minimization [38]	CART [34]
Training Data	10 × 200 μm and 10 × 250 μm	10 × 200 μm and 10 × 250 μm	10 × 200 μm and 10 × 250 μm	10 × 200 μm and 10 × 250 μm
No. of Iterations	5 (I-V), 20 (RF)	20 (I-V), 100 (RF)	30	40
Testing Data	10 × 220 μm	10 × 220 μm	10 × 220 μm	10 × 220 μm
Optimization Parameters	Consequent parameters (p_i, q_i, r_i)	Weights and Bias	C, σ, ϵ	Max. no. of splits, Minimum Leaf size, Tree Depth
Mapping	MF (Gaussian)	Activation Function (Tan-Sigmoid)	Gaussian kernel	Tree Graph
Model Type	Multiple Input Single Output	Multiple Input Multiple Output	Multiple Input Single Output	Multiple Input Single Output
Data Size Handling	Moderate	Massive	Moderate	Large

and can develop high-performance models for prediction. Generally, to estimate the mapping function, SVR and DT-based GaN HEMT models need comparatively more training data samples than ANN and ANFIS-based GaN HEMT models. ANN-based models have a definite structure, say a bunch of hidden layers with sizes h_1 through h_n depending on the number of features plus bias parameters [24], [25], [27], [28], [29] or ANFIS based model development of GaN

TABLE 7. Comparison of GaN HEMTs modeling approaches.

Parameters/ Model	Empirical / Angelov [16]-[23]	Physics ASM-HEMT, MVSG [7]-[15]	Machine Learning (ANN, SVR,DT) [24]-[34]	Hybrid Model [35]-[38] (Empirical or Physics + ML)	Proposed Model ANFIS
Framework	Self-derived equations	Theoretical Physics	Measured Data	Extracted Data from empirical or physics	Data and Set of Rules
Model Development	In between ML and proposed	Slowest	Fast	Fast	Fast
Process Information	Required	Limited	Required	Required	Required
DC and S-parameter Fitting	Good	Good	Good	Good	Good
Scalable	Yes but Limited	Completely	Yes / (Depends on data provided to the model)	Yes	Yes / (Depends on data provided to the model)
Large Signal accuracy at different bias	Not	Yes	Yes	Yes	Yes but needs investigation
Robustness	No	Yes	Yes	Yes	Yes
Tuning Parameters	Less than Physics based	Most	Few	Medium	Few

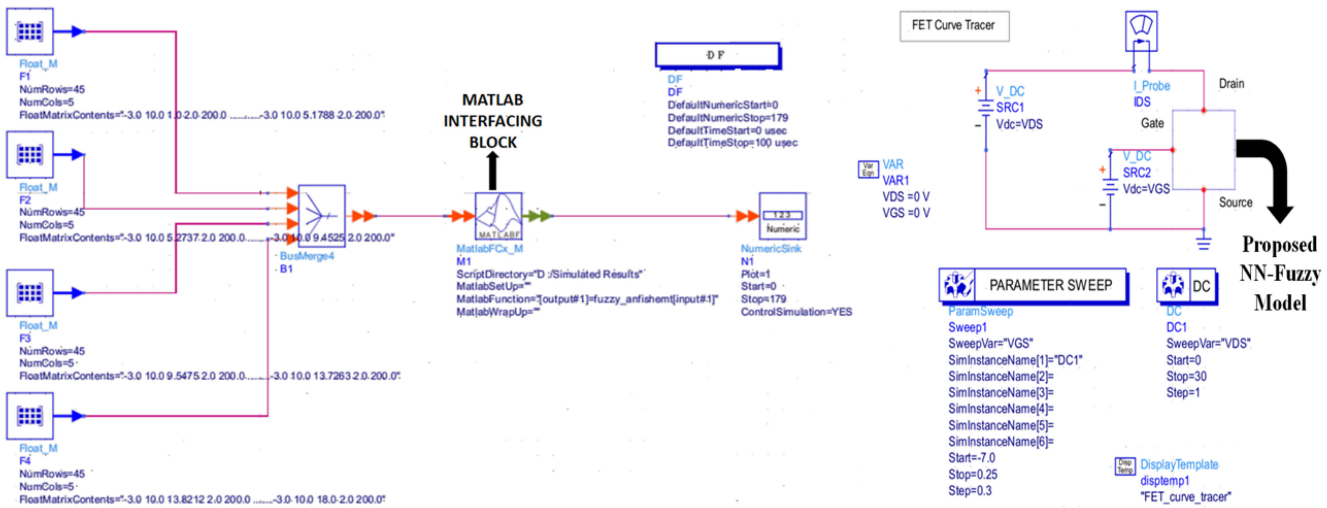

(a)

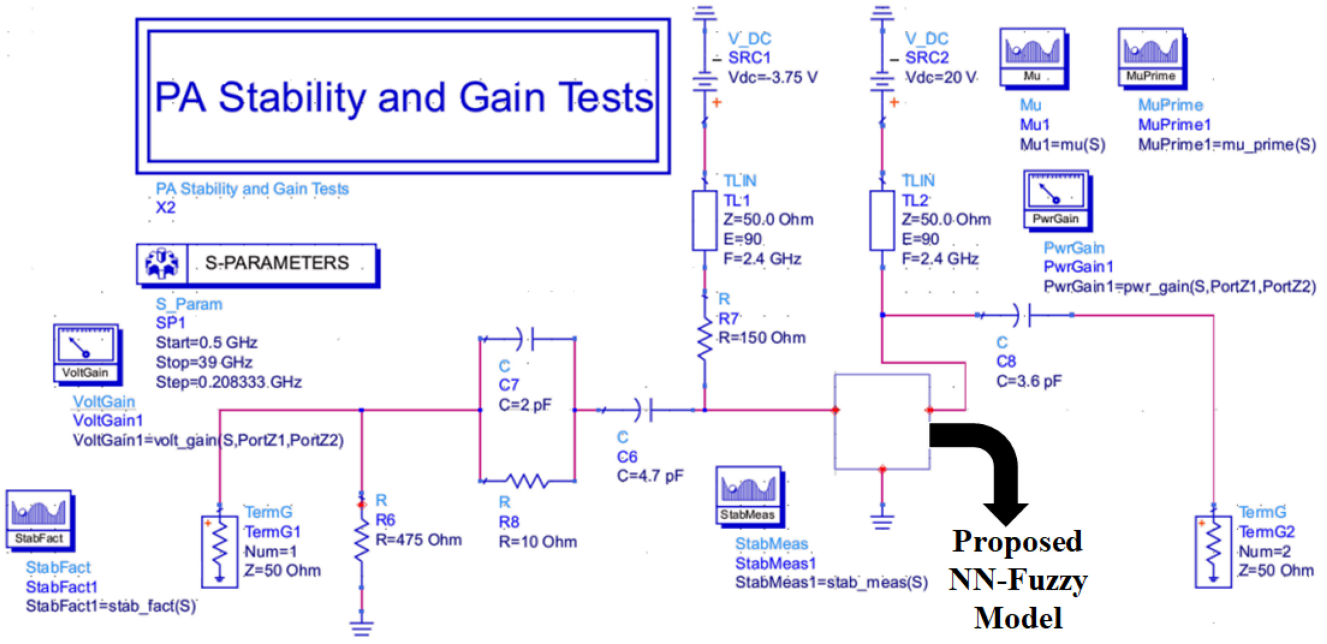

(b)

FIGURE 15. (a) MATLAB-ADS interfacing and I-V curve tracer, and (b) amplifier stability and gain test circuit using proposed models.

HEMTs have 5 stages as described in Fig. 3 and the MFs or rules associated with each variable. By contrast, an SVR (say at least a kernel) consists of a set of support vectors, selected from the training data, with a weight for each. In the worst scenario, the number of support vectors is exactly the number of training samples (though that mainly occurs with a small training dataset or in a degenerate situation) and in general its model size scales linearly [30], [31], [32], [33]. A similar concept applies to DT where the number of leaves and tree branches grow [34]. The training speed of SVR and DT-based models is relatively slower than ANN and ANFIS as they have far more parameters to train. SVR

TABLE 8. Comparison of MSE for all multi-bias conditions on the test device between the proposed ANFIS and various other ML techniques.

Performance/ Response	MSE (ANFIS) Proposed	MSE (ANN) [30] [31] [34] [38]	MSE (SVR) [32] [33] [45]	MSE (DT) [39]
$\|S_{11}\|$	3.28e-4	5.41e-4	6.38e-4	7.89e-5
$\angle S_{11}$	3.98e-4	7.68e-4	5.12e-3	4.23e-4
$\|S_{12}\|$	1.82e-3	8.5e-4	7.21e-3	6.23e-4
$\angle S_{12}$	2.87e-3	5.93e-3	6.31e-3	5.23e-3
$\|S_{21}\|$	3.37e-3	6.13e-4	6.8e-3	4.33e-3
$\angle S_{21}$	3.67e-3	3.72e-3	7.83e-3	5.12e-3
$\|S_{22}\|$	4.99e-4	6.23e-4	6.93e-4	2.23e-5
$\angle S_{22}$	2.93e-4	3.88e-4	1.3e-3	3.21e-3
I_{DS}	1.99e-4	1.13e-4	2.67e-4	1.67e-4
f_T	3.99e-4	2.23e-4	3.12e-4	4.68e-4
f_{max}	2.89e-4	2.03e-4	7.89e-4	3.75e-3
g_m	1.69e-4	1.653e-4	2.45e-2	4.45e-4
g_{ds}	1.29e-4	1.43e-4	9.35e-3	5.63e-3

and DT are more prone to overfit the training data and it is relatively harder to explain the possible reasons for the decision of specific predictions. ANN-based models often converge on local minima rather than global minima and often happens the same problem occurs with DTs. ANN-based models often deal with overfitting if training goes on for a longer period, i.e., ANN ANN-based training starts to consider the noise or outliers as a part of training. SVR and DTs-based models deal with outliers effectively. FL-based models are highly immune to noise and are the fastest to train with good generalization capability as can be seen in Table 6.

A new comparison among various modeling approaches, i.e., the proposed model and physics, empirical, ML-based is provided in Table 7 based on performance parameters. Compared to physical modeling, empirical modeling (including cold pinch-off), and hybrid modeling, the proposed model has the fewest parameters that need to be adjusted or optimized. As a result, model development is rapid. However, because they require the optimization or tuning of a broad range of parameters along with the solution of multiple algebraic and higher-order differential equations, analytical and empirical models require a comparatively longer development time [6], [7], [8], [9], [10], [11], [12], [13], [14], [15], [16], [17], [18], [19], [20], [21], [22], [23]. Empirical models have limited or lack scalability, for the same set of parameters cannot fit the model for different devices. Physics-based compact models are scalable and highly accurate [16], [17], [18], [19], [20], [21], [22], [23]. ML-based models can expedite the process with high prediction accuracy but do not guarantee scalability [24], [25], [26], [27], [28], [29], [30], [31], [32], [33], [34]. The proposed ANFIS modeling approach demonstrates scalability, high accuracy for DC and S-parameter fitting, good generalization capability, and rapid model development when compared to several ML techniques such as SVR and DT. However, the ANFIS-based modeling approach cannot handle when dealing with massive datasets leading to a decline in its generalization capability. This aspect needs to be explored and investigated. It is imperative to mention that the number of fuzzy rules can be reduced and accuracy can be made high at the same time by adopting a better way of clustering the data. The proposed Sugeno ANFIS-based GaN HEMTs models suffer from primary limitations such as a single Output system, zeroth, or first-order system which means all output membership functions must be of the same type, either linear or constant, different rules cannot use the same output MF, i.e., no. of output MF must be equal to no. of rules. This limitation may create a trade-off condition where the modeling engineer needs to consider more no. of fuzzy rules with good accuracy.

Eventually, the same measured data was used to develop the trained models using the ANN, SVR, and DT-based GaN HEMTs model. Further, the testing of the model was conducted on 10×220 μm device, and a comparison between the proposed approach and other modeling techniques based on test set error measured in terms of MSE has been shown in Table 8. ANN, SVR, and DT techniques have higher prediction accuracy but the proposed ANFIS modeling approach for GaN HEMTs has better generalization capability than all other ML techniques. It can be observed that the ANFIS-based proposed methodology shows a considerable improvement for various outputs on the test set.

III. DEPLOYMENT OF FUZZY BASED GaN HEMT MODEL

The next step is to demonstrate the utility of the proposed ANFIS-based models of GaN HEMTs for high-frequency circuit design. In this process, the primary step is to ensure seamless co-simulation and easy and fast execution of the behavioral model between MATLAB and Keysight's Advanced Design System (ADS). MATLAB co-simulation in the ADS Ptolemy environment aids in establishing the interface between MATLAB and ADS as shown in Fig. 15(a). To execute this, the ADS environment calls a function developed in MATLAB that takes test inputs and generates output using the sink. To facilitate, the Numeric MATLAB palette provides a co-simulation block, the numeric source provides a float matrix block for providing inputs, and the sink is used to record the output. The data flow (DF) controller provides simulation control to the proposed data-driven model. Since the input size of one set of multi-biasing for a broad frequency range includes 180 samples, numeric start and numeric stop in the DF controller is assigned 0 and 179 respectively. Since a single float matrix block may only accept a maximum of 50 input samples of a single complete data test sample at a time, four float matrix blocks are employed to supply inputs to the function being called. Bus merger combines all the inputs sequentially and sends the input to a co-simulation block at once. In our case, the function eventually converts the output to a touchstone file to facilitate easy execution of the circuit design. The interfacing circuit demonstrates the incorporation of the data-driven model in a CAD tool.

The ANFIS-based GaN HEMTs I-V and S-parameters models are used for amplifier design at 2.4 GHz as shown in Fig. 15(b). The presented design is for a 10×220 μm device, biased at a quiescent bias point of V_{GS}=−3.75 V, V_{DS}=20 V using I-V curve Tracer. Stability parameters based on the Rollett stability criteria ($K-\Delta$ and μ test) are calculated for

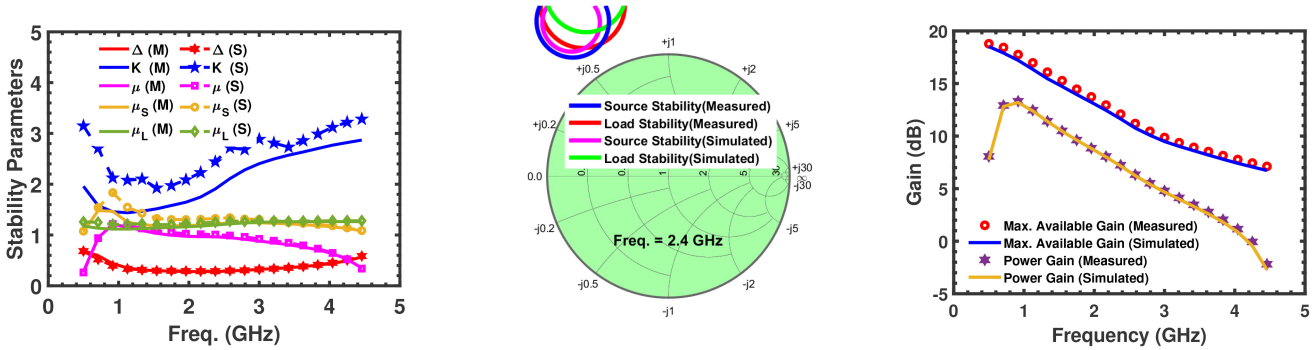

FIGURE 16. (a) Stability test parameters, (b) stability circles at 2.4 GHz, and (c) small-signal gain of the amplifier for the inputs $V_{GS} = -2.5$ V; $V_{DS} = 20$ V.

the amplifier. It is evident from Fig. 16(a) that $K > 1$, $\delta < 1$, $\mu > 0$, which implies that the amplifier is unconditionally stable over the design frequency range [49]. It is apparent from Fig. 16(b) that the stability circles are outside the Smith Chart at both the source and the load end, which validates the amplifier's stability. Eventually, the small-signal gain and power gain of the amplifier at 2.4 GHz are found to be 14 dB and 9.5 dB respectively, as shown in Fig. 16(c).

IV. CONCLUSION

A novel methodology has been presented based on the application of ANFIS for modeling non-linear RF/microwave semiconductor devices. SC-based ANFIS model technique is proposed to model the I-V characteristics, S-parameters, and RF performance parameters of GaN HEMTs. The most optimized parameter set of fuzzy models which provides the highest accuracy with the least number of fuzzy rules or MFs is selected to model the GaN HEMTs device. The developed ANFIS-based models are further tested on devices of geometries $10 \times 220\,\mu$m, $2 \times 200\,\mu$m and $4 \times 100\,\mu$m for a wide range of multi-bias conditions and a broad frequency range to manifest interpolation and extrapolation accuracy of the proposed modeling technique. The excellent modeling accuracy obtained for three different transistors of distinct dimensions for the same set of premise (antecedent) parameter values aids in establishing width-scalable GaN HEMTs behavioral models. We also demonstrated the utility of the proposed models in amplifier circuit design. The proposed ANFIS models add new dimensions to the contemporary modeling approaches for semiconductor devices and can be further extended to investigate the feasibility of large signal modeling of GaN HEMTs.

ACKNOWLEDGMENT

The authors thank the Nano LAB, Department of Electrical Engineering, IIT Kanpur, and the Head of the Lab Prof. Chauhan for providing access to their measurement facility and the GaN HEMT measurement data.

REFERENCES

[1] Y. S. Noh and I. B. Yom, "A linear GaN high power amplifier MMIC for Ka-band satellite communications, *IEEE Microw. Wireless Compon. Lett.*, vol. 26, no. 8, pp. 619–621, Aug. 2016.

[2] M. S. Hashmi, Z. S. Rogojan, and F. M. Ghannouchi, "A flexible dual-inflection point RF pre-distortion linearizer for microwave power amplifiers," *Progr. Electromagn. Res. C*, vol. 13, pp. 1–18, Apr. 2010.

[3] A. M. Zaidi, T. Khan, M. T. Beg, B. K. Kanaujia, and K. Rambabu, "Dual-band design techniques for microwave passive circuits: A review and applications," *IEEE Microw. Mag.*, vol. 23, no. 7, pp. 61–77, Jul. 2022.

[4] M. S. Hashmi, A. L. Clarke, S. P. Woodington, J. Lees, J. Benedikt, and P. J. Tasker, "Electronic multi-harmonic load-pull system for experimentally driven power amplifier design optimization," in *IEEE MTT-S Int. Microw. Symp. Dig.*, Boston, MA, USA, Jun. 2009, pp. 1549–1552.

[5] L. Sang, Y. Xu, Y. Wu, and R. Chen, "Device and compact circuit-level modeling of graphene field-effect transistors for RF and microwave applications," *IEEE Trans. Circuits Syst. I, Reg. Paper*, vol. 65, no. 8, pp. 2559–2570, Aug. 2018.

[6] A. R. Alt, D. Marti, and C. R. Bolognesi, "Transistor modeling: Robust small-signal equivalent circuit extraction in various HEMT technologies," *IEEE Microw. Mag.*, vol. 14, no. 4, pp. 83–101, Jun. 2013.

[7] S. A. Albahrani, L. Heuken, D. Schwantuschke, T. Gneiting, J. N. Burghartz, and S. Khandelwal, "Consistent surface-potential-based modeling of drain and gate currents in AlGaN/GaN HEMTs," *IEEE Trans. Electron Devices*, vol. 67, no. 2, pp. 455–462, Feb. 2020.

[8] S. Ghosh et al., "Surface-potential-based compact modeling of gate current in AlGaN/GaN HEMTs," *IEEE Trans. Electron Devices*, vol. 62, no. 2, pp. 443–448, Feb. 2015.

[9] A. Pampori et al., "Modeling of bias-dependent effective velocity and its impact on saturation transconductance in AlGaN/GaN HEMTs," *IEEE Trans. Electron Devices*, vol. 68, no. 7, pp. 3302–3307, Jul. 2021.

[10] M. Pradhan et al., "Physical modeling of charge trapping effects in GaN/Si devices and incorporation in the ASM-HEMT model," *IEEE J. Electron Devices Soc.*, vol. 9, pp. 748–755, 2021.

[11] N. C. Miller, A. Brown, M. Elliott, and R. Gilbert, "Temperature dependent large-signal modeling of GaN HEMTs at Ka-band using the ASM-HEMT," in *Proc. IEEE Wireless Microw. Technol. Conf. (WAMICON)*, Melbourne, FL, USA, 2023, pp. 21–24.

[12] S. Ma, J. Liu, J. Wang, and Y. Xia, "Comparison of two standard physical models of GaN HEMTs: MVSG and ASM," in *Proc. IEEE MTT-S Int. Wireless Symp. (IWS)*, Nanjing, China, 2021, pp. 1–3.

[13] U. Radhakrishna et al., "Facilitation of GaN-based RF and HV-circuit designs using MVS-GaN HEMT compact model," *IEEE Trans. Electron Devices*, vol. 66, no. 1, pp. 95–105, Jan. 2019.

[14] R. Fang, Y. Feng, J. Chong, K. Chan, U. Radhakrishna, and L. We, "Comprehensive MVSG compact model for power GaN devices," in *Proc. 35th Int. Symp. Power Semicond. Devices ICs (ISPSD)*, 2023, pp. 123–126.

[15] R. Fang, D. Ma, U. Radhakrishna, and L. Wei, "MVSG GaN-HEMT model: Approach to simulate fringing field capacitances, gate current de-biasing, and charge trapping effects," in *Proc. IEEE BiCMOS Compound Semicond. Integr. Circuits Technol. Symp.*, Phoenix, AZ, USA, 2022, pp. 21–24.
[16] S. A. Ahsan, A. U. H. Pampori, S. Ghosh, S. Khandelwal, and Y. S. Chauhan, "A new small-signal parameter extraction technique for large gate-periphery GaN HEMTs," *IEEE Microw. Wireless Compon. Lett.*, vol. 27, no. 10, pp. 918–920, Oct. 2017.
[17] Y. Chen, R. Xu, and Y. Xu, "A simplified Angelov self-heating modeling using short and long duration Pulsed I-V measurement for a GaN HEMT," in *Proc. IEEE MTT-S Int. Wireless Symp. (IWS)*, Shanghai, China, 2020, pp. 1–3.
[18] S. Emekar et al., "Modified Angelov model for an exploratory GaN-HEMT technology with short, few-fingered gates," in *Proc. Int. Conf. Simulat. Semicond. Processes Devices (SISPAD)*, Kamakura, Japan, 2017, pp. 117–120.
[19] G.P. Gibiino, A. Santarelli, and F. Fillicori, "A GaN HEMT global large-signal model including charge trapping for multibias operation," *IEEE Trans. Microw. Theory Techn.*, vol. 66, no. 11, pp. 4684–4697, Nov. 2018.
[20] A. Jarndal, R. Essaadali, and A. B. Kouki, "A reliable model parameter extraction method applied to AlGaN/GaN HEMTs," *IEEE Trans. Comput. Aided Design Integr. Circuits Syst.*, vol. 35, no. 2, pp. 211–219, Feb. 2016.
[21] G. Crupi et al., "High-frequency extraction of the extrinsic capacitances for GaN HEMT technology," *IEEE Microw. Wireless Compon. Lett.*, vol. 21, no. 8, pp. 445–447, Aug. 2011.
[22] A. Khusro, M. S. Hashmi, A. Q. Ansari, A. Mishra, and M. Tarique, "An accurate and simplified small signal parameter extraction method for GaN HEMT," *Int. J. Circuit Theory Appl.*, vol. 47, no. 6, pp. 941–953, 2019.
[23] X. Zhao et al., "Temperature-dependent access resistances in large-signal modeling of millimeter-wave AlGaN/GaN HEMTs," *IEEE Trans. Microw. Theory Techn.*, vol. 65, no. 7, pp. 2271–2278, Jul. 2017.
[24] S. Husain, M. Hashmi, and F. M. Ghannouchi, "Comprehensive investigation and comparative analysis of machine learning-based small-signal modelling techniques for GaN HEMTs," *IEEE J. Electron Devices Soc.*, vol. 10, pp. 1015–1032, 2022.
[25] A. Jarndal, S. Husain, M. Hashmi, and F. M. Ghannouchi, "Large-signal modeling of GaN HEMTs using hybrid GA-ANN, PSO-SVR, and GPR-based approaches," *IEEE J. Electron Devices Soc.*, vol. 9, pp. 195–208, 2021.
[26] J. Cai et al., "Bayesian inference-based behavioral modeling technique for GaN HEMTs," *IEEE Trans. Microw. Theory Techn.*, vol. 67, no. 6, pp. 2291–2301, Jun. 2019.
[27] A. Khusro, S. Husain, M. S. Hashmi, and A. Q. Ansari, "Small signal behavioral modeling technique of GaN high electron mobility transistor using artificial neural network: An accurate, fast, and reliable approach," *Int. J. RF Microw. Comput.-Aided Eng.*, vol. 30, no. 4, 2020, Art. no. e22112.
[28] Z. Marinkovic, G. Crupi, A. Caddemi, and V. Markovic, "GaN HEMT small-signal modeling: Neural networks versus equivalent circuit," in *Proc. IEEE 30th Int. Conf. Microelectron.*, 2017, pp. 153–156.
[29] A. D. Huang, Z. Zhong, W. Wu, and Y.-X. Guo, "An artificial neural network-based electrothermal model for GaN HEMTs with dynamic trapping effects consideration," *IEEE Trans. Microw. Theory Techn.*, vol. 64, no. 8, pp. 2519–2528, Aug. 2016.
[30] M. Q. Geng et al., "Modified small-signal behavioral model for GaN HEMTs based on support vector regression," *Int. J. RF Microw. Comput.-Aided Eng.*, vol. 31, no. 9, 2021, Art. no. e22774.
[31] J. Cai, J. King, C. Yu, J. Liu, and L. Sun, "Support vector regression-based behavioral modeling technique for RF power transistors,"*IEEE Microw. Wireless Compon. Lett.*, vol. 28, no. 5, pp. 428–430, May 2018.
[32] A. Khusro, S. Husain, M. S. Hashmi, A. Q. Ansari, and S. Arzykulov, "A generic and efficient globalized kernel mapping-based small-signal behavioral modeling for GaN HEMT," *IEEE Access*, vol. 8, pp. 195046–195061, 2020.
[33] A. Khusro, M. S. Hashmi, and A. Q. Ansari, "Exploring support vector regression for modeling of GaN HEMT," in *Proc. IEEE MTT-S Int. Microw. RF Conf. (IMaRC)*, Kolkata, India, 2018, pp. 1–3.
[34] A. Khusro, M. S. Hashmi, A. Q. Ansari, and M. Auyenur, "A new and reliable decision tree based small-signal behavioral modeling of GaN HEMT," in *Proc. IEEE 62nd Int. Midwest Symp. Circuits Syst. (MWSCAS)*, Dallas, TX, USA, 2019, pp. 303–306.
[35] F. Chavez, D. T. Davis, N. C. Miller, and S. Khandelwal, "Deep learning-based ASM-HEMT I-V parameter extraction," *IEEE Electron Device Lett.*, vol. 43, no. 10, pp. 1633–1636, Oct. 2022.
[36] M. Yusuf et al., "A deep learning space mapping based enhancement of compact models for accurate prediction of trapping in GaN HEMTs from DC to mm-Wave frequency," in *IEEE MTT-S Int. Microw. Symp. (IMS)*, San Diego, CA, USA, Jun. 2023, pp. 89–92..
[37] H. Luo, X. Yan, J. Zhang, and Y. Guo, "A neural network-based hybrid physical model for GaN HEMTs," *IEEE Trans. Microw. Theory Techn.*, vol. 70, no. 11, pp. 4816–4826, Nov. 2022.
[38] A. Khusro, M. S. Hashmi, and A. Q. Ansari, "Enabling the development of accurate intrinsic parameter extraction model for GaN HEMT using support vector regression (SVR)," *IET Microw., Antennas Propag.*, vol. 30, no. 9, pp. 1457–1466, 2019.
[39] H.-X. Li and C. L. P. Chen, "The equivalence between fuzzy logic systems and feedforward neural networks," *IEEE Trans. Neural Netw.*, vol. 11, no. 2, pp. 356–365, Mar. 2000.
[40] R. Babuska, "Fuzzy modeling and identification," Ph.D. dissertation, Dept. Electr. Eng., Tech. Univ. Delft, Delft, The Netherlands, Jan. 1997.
[41] J. Zhai, J. Zhou, L. Zhang, J. Zhao, and W. Hong, "The dynamic behavioral model of RF power amplifiers with the modified ANFIS," *IEEE Trans. Microw. Theory Techn.*, vol. 57, no. 1, pp. 27–35, Jan. 2009.
[42] J. Zhai, J. Zhou, L. Zhang, J. Zhao, and W. Hong, "Dynamic behavioral modeling of power amplifiers using ANFIS-based Hammerstein," *IEEE Microw. Wireless Compon. Lett.*, vol. 18, no. 10, pp. 704–706, Oct.2008.
[43] B. Chatterjee, D. Shoemaker, H. Wong, and S. Choi, "AlGaN/GaN HEMT device physics and electrothermal modeling,"*Thermal Management of Gallium Nitride Electronics* (Woodhead Publishing Series in Electronic and Optical Materials). Washington DC, USA: Elsevier, 2022, pp. 103–163.
[44] S. Chiu, "Method and software for extracting fuzzy classification rules by subtractive clustering," in *Proc. North Amer. Fuzzy Inf. Process.*, Berkeley, CA, USA, 1996, pp. 461–465.
[45] T. Cavdar, "PSO tuned ANFIS equalizer based on fuzzy C-means clustering algorithm," *AEU-Int. J. Electron. Commun.*, vol. 70, no. 6, pp. 799–807, 2016.
[46] S. L. Chiu, "Fuzzy model identification based on cluster estimation," *J. Intell. Fuzzy Syst.*, vol. 2, no. 3, pp. 267–78, 1994.
[47] G. Crupi et al., "An extensive experimental analysis of the kink effects in S_{22} and h_{21} for a GaN HEMT," *IEEE Trans. Microw. Theory Techn.*, vol. 62, no. 3, pp. 513–520, Mar. 2014.
[48] C. Roff et al., "Analysis of DC–RF dispersion in AlGaN/GaN HFETs using RF waveform engineering," *IEEE Trans. Electron Devices*, vol. 56, no. 1, pp. 13–19, Jan. 2009.
[49] D. M. Pozar, *Microwave Engineering*, Hoboken, NJ, USA: Wiley, 2012.